Interface structure governed by plastic and structural dissimilarity in perovskite La 0.7 Sr 0.3 MnO 3 nanodots on rock-salt MgO substrates

P. Abellan, J. Zabaleta, J. Santiso, Marie-José Casanove, N. Dix, J. Aguiar, N. Browning, N. Mestres, T. Puig, X. Obradors, et al.

Interface structure governed by plastic and structural dissimilarity in *perovskite* $La_{0.7}Sr_{0.3}MnO_3$ nanodots on *rock-salt* MgO substrates

Cite as: Appl. Phys. Lett. **100**, 083104 (2012); https://doi.org/10.1063/1.3687692
Submitted: 28 October 2011 . Accepted: 01 February 2012 . Published Online: 22 February 2012

P. Abellán, J. Zabaleta, J. Santiso, M.-J. Casanove, N. Dix, J. Aguiar, N. D. Browning, N. Mestres, T. Puig, X. Obradors, and F. Sandiumenge

Interface structure governed by plastic and structural dissimilarity in *perovskite* $La_{0.7}Sr_{0.3}MnO_3$ nanodots on *rock-salt* MgO substrates

P. Abellán,[1,a)] J. Zabaleta,[2] J. Santiso,[3] M.-J. Casanove,[4] N. Dix,[2] J. Aguiar,[1,5] N. D. Browning,[1] N. Mestres,[2] T. Puig,[2] X. Obradors,[2] and F. Sandiumenge[2,b),c)]

[1]*Department of Chemical Engineering and Materials Science, University of California—Davis, Davis, California 95616, USA*

[2]*Institut de Ciència de Materials de Barcelona, CSIC, Campus de la Universitat Autònoma de Barcelona, 08193 Bellaterra, Catalonia, Spain*

[3]*Research Centre for Nanoscience and Nanotechnology, CIN2 (CSIC-ICN), Campus UAB, 08193 Bellaterra, Catalonia, Spain*

[4]*CNRS, CEMES (Centre d'Elaboration de Matériaux et d'Etudes Structurales), BP 94347, 29 Rue Jeanne Marvig, F-31055 Toulouse, France*

[5]*Condensed Matter and Materials Division, Lawrence Livermore National Laboratory, Livermore, California 37831-6064, USA*

(Received 28 October 2011; accepted 1 February 2012; published online 22 February 2012)

Self-assembled $La_{0.7}Sr_{0.3}MnO_3$ perovskite nanodots have been grown on highly mismatched rock-salt type MgO substrates by chemical solution deposition. The interfacial dislocation structure indicates that the relaxation mechanism is governed by the easy glide of MgO $1/2\langle 101\rangle\{101\}$ dislocations towards the interface, where they dissociate into misfit-relieving and tilting components. The latter induce a 4-domain tilt pattern superimposed to the main cube-on-cube epitaxial orientation. It is shown that the inheritance of the rotational component of the Burgers vector has detrimental consequences on the interfacial quality, evidencing the impact of structural and plastic dissimilarity on the design of self-assembled nanostructures. © *2012 American Institute of Physics*. [doi:10.1063/1.3687692]

Size reduction of perovskite-based magnetic nanostructures is a necessary step towards the development of spin-based applications. While top-down approaches hardly allow patterning of oxide nanostructures below 100 nm,[1] bottom-up strategies offer a unique opportunity to overcome this limitation. Self-assembling processes arising from lattice misfit, however, are governed by a balance between elastic strain, surface, and interface energies,[2] nowadays mostly established for conventional semiconductor systems.[3] Much less effort has been devoted to take advantage of self-assembling phenomena in the case of oxides. Notably, the atomic scale microstructural pathway satisfying this energy balance appears specific of the involved crystal structures and determines the functionality of the resulting nanostructure. Establishing a correlation between misfit relaxation mechanisms and different interfacial scenarios thus becomes essential to produce self-assembled oxide nanostructures in a predictive way. Among deposition techniques, chemical solution deposition (CSD) is emerging as a high-throughput growth technique that has already been proved efficient for the preparation of nanostructures of a variety of complex oxide materials.[4,5] Here, we present a structural analysis of the perovskite/rock-salt interface between $La_{0.7}Sr_{0.3}MnO_3$ (LSMO) and the MgO substrate, in order to get insights into the role of plastic and structural dissimilarity on the development of interfacial structures.

LSMO nanoislands on (001) oriented MgO substrates were obtained by CSD from solutions of the metal propionates in propionic acid[6] and subsequent annealing at 900 °C under oxygen atmosphere for 1-3 h. Fig. 1(a) is an atomic force microscopy (AFM) image, obtained in the dynamic mode, of the LSMO nanodot-decorated (001)-MgO surface, showing homogeneous spatial and size distributions. A quantitative analysis indicates a broader distribution for equivalent island diameters $\langle D\rangle = 50 \pm 20$ nm than for island heights $\langle h\rangle = 7 \pm 2$ nm (Fig. 1(b)). A higher magnification image resolving the MgO surface topography reveals unit cell high steps aligned with the $\langle 110\rangle$-MgO directions (Fig. 1(c)). Most of the nanodots reside at kink sites and step edges with the basal sides aligned with the steps. This morphology suggests that LSMO nanodots preferentially nucleated at kink sites and grew by diffusion of adatoms along the steps edges. Since the LSMO nanodots hold a cube-on-cube orientation relative to the MgO (see x-ray diffraction (XRD) pole-figure, Fig. 2(a)), it can be inferred by inspection of high resolution transmission electron microscopy (HRTEM) (see below, Fig. 3(a)) that the growth mechanism constrains the lateral facets of the nanodots to combinations of {110} and {111} planes, truncated by larger (001) top facets. The growth rate anisotropy inferred from the high aspect ratio $D/h \sim 7$ is not clearly understood. There are no surface energy determinations for different facets of LSMO. For the $La_{1-x}Ca_xMnO_3$ solid solution, however, a similar or slightly higher energy of the {001} facets compared with {110} ones has been estimated depending on x and atomic termination.[7] Assuming a similar behavior for

[a)]This research was partly performed while P.A. was at Institut de Ciència de Materials de Barcelona, CSIC, Campus de la Universitat Autònoma de Barcelona, 08193 Bellaterra, Catalonia, Spain.

[b)]This research was partly performed while F.S. was on sabbatical stay at the Department of Chemical Engineering and Materials Science, University of California—Davis, Davis, California 95616, USA.

[c)]Author to whom correspondence should be addressed. Electronic mail: felip@icmab.es.

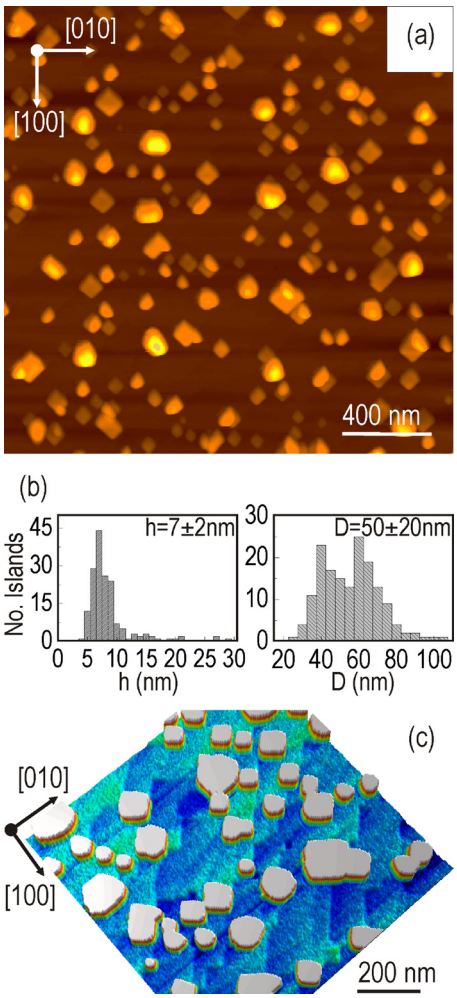

FIG. 1. (Color online) LSMO-nanodot/MgO template morphology. (a) Topographic AFM image of the LSMO/MgO nanostructure; z scale: 40 nm. (b) Diameter and height distribution histograms of LSMO nanodots. (c) AFM image showing the preferential location of the nanodots at kink sites along steps aligned with ⟨110⟩ azimuths. The nanodots exhibit a square base with edges aligned with the substrate steps.

LSMO, it is thus likely that the shape of the nanodots is kinetically determined by an enhancement of the lateral growth rate favored by the high degree of misfit strain relaxation achieved by the dislocation mechanism (see below) from the very early growth stages.[8]

Close inspection of the fine structure of the {101}-LSMO-poles (see inset in Fig. 2(a)) reveals that each pole is associated to four satellites lying along the [110] and [1-10] directions, indicating the occurrence of four additional orientation domains related to the precise cube-on-cube orientation by 2° to 5° tilts about the [110] and [1-10] axes. In order to determine the average in-plane strain state of the nanodots ensemble, we conducted XRD ϕ - $2\theta/\omega$ space mapping (ϕ is the azimuthal orientation) at a grazing incidence angle of 0.5° around the (200)-MgO and (200)-LSMO reflections using a conventional in-house Cu-Kα_1 source (see inset to Fig. 2(b)). Using $a_{MgO} = 4.21$ Å (Ref. 9) as a reference, a fit of peak positions in the corresponding $2\theta/\omega$ scan (Fig. 2(b)) yields an in-plane lattice parameter $a_{LSMO} = 3.876 \pm 0.006$ Å (bulk value $a_{LSMO} = 3.876$ Å (Ref. 10)), indicating a full relaxation of the misfit strain $\delta = (a_{MgO} - a_{LSMO})/a_{LSMO} = 0.086$.

Fig. 3(a) is a cross-section HRTEM image of a typical LSMO nanodot viewed along the [100] zone axis, obtained in a *Cs*-corrected Tecnai F20 electron microscope operated at 200 kV at $Cs = -455.7$ nm and a defocus value $\Delta f = +13$ nm. From inspection of contrast variations, it can be inferred that the nanodot exhibits three facets: a central one inclined to [100] (viewing direction) and [001] (perpendicular to the substrate), and two side ones inclined to [100], [010], and [001]. The *apparent* inclination angle of the two side facets to [001] is 45°. We, therefore, assign (101), (1-11), and (111) to the lateral facets and (001) to the top one. The location and character of interfacial dislocations labeled **1** to **7** is indicated. Interfacial dislocation core structures are shown in an enlarged image of the boxed area in (a) comprising dislocations **3**, **4**, and **5** (Fig. 3(b)). Closure failures of Burgers circuits yield projected Burgers vectors $\mathbf{b}(\mathbf{3}) = \frac{1}{2}[011]$ and $\mathbf{b}(\mathbf{4}) = \mathbf{b}(\mathbf{5}) = \frac{1}{2}[010]$. The image shows that dislocation **3** has an extended core with partials $\mathbf{b}|| = \frac{1}{2}[010]$ and $\mathbf{b}^{\perp} = \frac{1}{2}[001]$, while **4** and **5** are single dislocations with Burgers vector of the type $\mathbf{b}||$. Severe bending of atomic planes is clearly observed in the neighborhood of dislocation **3** as a result of $\mathbf{b}^{\perp}$. The dislocation structure is thus similar to that observed in other perovskite/MgO heterostructures ($SrTiO_3$, $PbTiO_3$, $Ba_{0.6}Sr_{0.4}TiO_3$, and $BaZrO_3$ (Refs. 11–13)) and contrasts with Burgers vectors $\mathbf{b} = \langle 010 \rangle$ typically reported for LSMO films on perovskite substrates.[14–16]

Noticing that $\frac{1}{2}\langle 011 \rangle \{011\}$ is the most prominent glide system in the rock-salt structure,[17] and that LSMO is stiffer than MgO,[18,19] a likely mechanism to explain our observations is that $\frac{1}{2}\langle 011 \rangle$ dislocations are inherited from the substrate, as often observed in semiconductor heterostructures.[20] Accordingly, dislocations would reach the interface by gliding on MgO {011} planes intersecting the interface at 45°. Once at the interface, such dislocations would dissociate into a misfit relieving component $\mathbf{b}||$, glissile on the interface plane, and a $\mathbf{b}^{\perp}$ rotation component. The latter one introduces an $a_{MgO}/2[001]$ interfacial step thereby increasing the interfacial roughness. Analysis of the interface of 13 nanodots indicates that as a general trend $\mathbf{b}||$ dislocations outnumber $\mathbf{b}^{\perp}$ ones. This suggests that once dissociated, $\mathbf{b}^{\perp}$ dislocations tend to annihilate. The process can be visualized considering two $\frac{1}{2}\langle 011 \rangle$ dislocations reaching the interface by gliding on the (0-11) and (011) planes. After dissociation, the resulting two $\mathbf{b}^{\perp}$ partials have opposite signs and can cancel each other by a climb movement on the interface plane. These dislocation reactions would generate the irregular concave shape of the interface observed in Fig. 3(a). Conversely, glide of $\mathbf{b}^{\perp}$ partials on the (010) plane normal to the interface towards the surface of the nanodot seems unlikely because this movement would leave an antiphase boundary on the glide plane which has not been observed. Though the driving force for the annihilation of the $\mathbf{b}^{\perp}$ partials is not fully understood, we believe that it constitutes a selection mechanism of dislocations with the same sign which minimizes opposite tilts within the same nanodot. In addition, it reduces the tensile misfit strain. It is worth emphasizing that the observed interfacial structure is determined by the confluence of plastic and structural dissimilarities which favors the inheritance of dislocations which do not belong to the

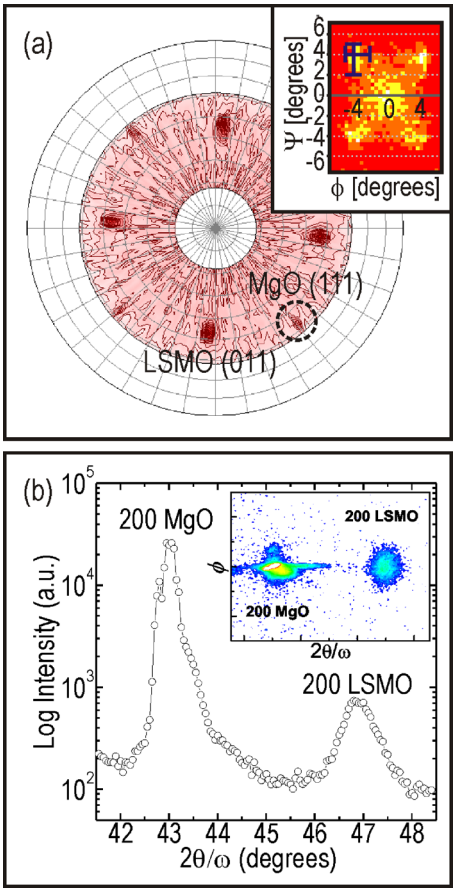

FIG. 2. (Color online) Average epitaxial orientation and degree of misfit relaxation of LSMO-nanodot/MgO. (a) Combined XRD pole-figures of the {111}-MgO and {110}-LSMO planes. Inset shows detailed scans around the {110}-LSMO pole showing splitting along the two mutually perpendicular ⟨110⟩ in-plane directions. The central peak corresponds to the precise cube-on-cube epitaxial orientation. (b) XRD grazing incidence $2\theta/\omega$ scans around the (200)-MgO and (200)-LSMO reflections. Inset shows the ϕ - $2\theta/\omega$ space map from which the linear scans were obtained by integrating over a phi-range enclosing all the diffracted intensity.

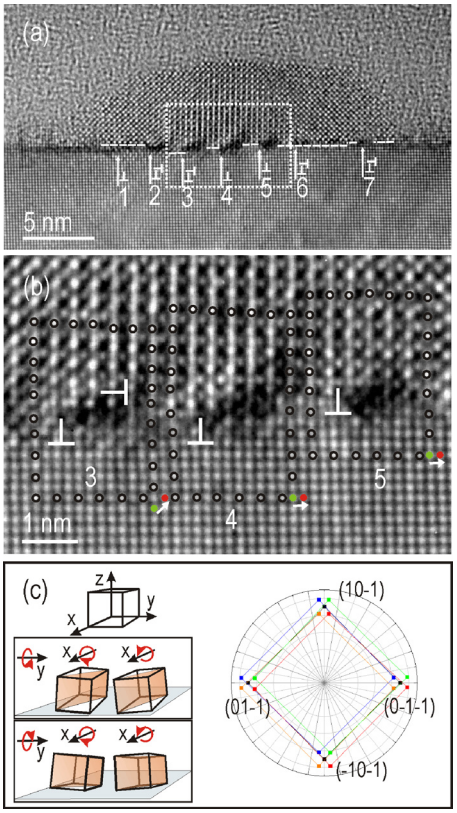

FIG. 3. (Color online) HRTEM analysis of the dislocation structures at the LSMO-nanodot/MgO interface. (a) LSMO nanodot viewed along the [100] zone axis, exhibiting a highly dislocated interface. (b) Enlarged image of the area boxed in (a) showing the core structures of the two types of partial dislocations found at the interface, with $\mathbf{b}^{\parallel} = \frac{1}{2}[100]$ and $\mathbf{b}^{\perp} = \frac{1}{2}[001]$, as obtained from the Burgers circuits drawn in the image. (c) Schematic illustration of tilts associated to a square array of interfacial $\mathbf{b}^{\perp}$ dislocations and calculated pole figures displaying a similar rotation domain structure as the one measured.

primary slip system of the nanodots. The features of the dislocation structure evidence that the "as-inherited" configuration is unstable and evolves to decrease its strain energy. However, topological constrains impede the complete annihilation of the undesired rotational $\mathbf{b}^{\perp}$ partials, resulting in severe residual strains as can readily be appreciated by direct inspection of HRTEM images (see Figs. 3(a) and 3(b)), which would be absent if the misfit was accommodated by dislocations belonging to the nanodot.

Turning now to the correlation between the average domain pattern revealed in the pole-figure (inset in Fig. 2(a)) and the interfacial dislocation structure, it is straightforward to see that the [100] and [010] tilts induced by two orthogonal sets of $\mathbf{b}^{\perp}$ dislocations result in a net rotation about the in-plane ⟨110⟩ directions. Taking into account the two possible tilt senses, the four satellite {101}-LSMO poles are reproduced, as depicted in Fig. 3(c). The higher intensity of the main central poles, on the other hand, indicates that a significant volume fraction of LSMO still adopts a precise cube-on-cube epitaxial association with the substrate.

In summary, the LSMO-nanodot/MgO interface is shown to be inherently rough and defective as a consequence of the interfacial behavior of misfit dislocations inherited from the substrate. The present results highlight the role of structural and plastic dissimilarity in determining the interfacial quality of self-assembled functional nanostructures.

We acknowledge the financial support from MEC (Consolider NANOSELECT, MAT2008-01022, MAT2011-29081-C02-02, and FPU; F.S. acknowledges a sabbatical stay at UC-Davis) and Generalitat de Catalunya (Pla de Recerca 2009-SGR-770 and XaRMAE). The Cs-corrected Tecnai-F20 FEI electron microscope was used in the framework of the European project ESTEEM (contract 026019).

[1]D. Ruzmetov, Y. Seo, L. J. Belenky, D.-M. Kim, X. Ke, H. Sun, V. Chandrasekhar, C.-B. Eom, M. S. Rzchowski, and X. Pan, Adv. Mater. **17**, 2869 (2005).
[2]J. V. Barth, G. Costantini, and K. Kern, Nature (London) **437**, 671 (2005).
[3]J. Stangl, V. Holy, and G. Bauer, Rev. Mod. Phys. **76**, 725 (2005).
[4]M. Gibert, T. Puig, X. Obradors, A. Benedetti, F. Sandiumenge, and R. Hühne, Adv. Mater. **19**, 3937 (2007).
[5]A. Carretero-Genevrier, N. Mestres, T. Puig, A. Hassini, J. Oró, A. Pomar, F. Sandiumenge, X. Obradors, and E. Ferain, Adv. Mater. **20**, 3672 (2008).
[6]U. Hasenkox, C. Mitze, R. Waser, R. R. Arons, J. Pommer, and G. Guntherodt, J Electroceram. **3**, 255 (1999).
[7]M. J. Akhtar, C. R. A. Catlow, B. Slater, A. M. Walker, and S. M. Woodley, Chem. Mater. **18**, 1559 (2006).
[8]P. Müller and R. Kern, Surf. Sci. **457**, 229 (2000).
[9]V. G. Tsirelson, A. S. Avilov, Y. A. Abramov, E. L. Belokoneva, R. Kitaneh, and D. Feil, Acta Crystallogr. **54**, 8 (1998).

[10]M. C. Martin, G. Shirane, Y. Endoh, K. Hirota, Y. Morimoto, and Y. Tokura, Phys. Rev. B **53**, 14285 (1996).
[11]S. Stemmer, S. K. Streiffer, F. Ernst, and M. Rühle. Phys. Status Solidi A **147**, 135 (1995).
[12]J. C. Jiang, Y. Lin, C. L. Chen, C. W. Chu, and E. I. Meletis, J. Appl. Phys. **91**, 3188 (2002).
[13]S. B. Mi, C. L. Jia, M. I. Faley, U. Poppe, and K. Urban, J. Cryst. Growth **300**, 478 (2007).
[14]X. Y. Qi, J. Miao, X. F. Duan, and B. R. Zhao, J. Cryst. Growth **277**, 218 (2005).
[15]M. J. Zhuo, Y. L. Zhu, and X. L. Ma, Philos. Mag. Lett. **86**, 469 (2006).
[16]O. I. Lebedev, G. Van Tendeloo, S. Amelinckx, H. L. Ju, and K. M. Krishnan, Philos. Mag. A **80**, 673 (2000).
[17]Ph. Carrez, D. Ferré, and P. Cordier, Modell. Simul. Mater. Sci. Eng. **17**, 035010 (2009).
[18]T. W. Darling, A. Migliori, E. G. Moshopoulou, S. A. Trugman, J. J. Neumeier, J. L. Sarrao, A. R. Bishop, and J. D. Thompson, Phys. Rev. B. **57**, 5093 (1998).
[19]D. Cáceres, I. Vergara, R. González, and Y. Chen, Philos. Mag. A **82**, 1159 (2002).
[20]N. Guelton, R. G. Saint-Jacques, G. Lalande, and J.-P. Dodelet, J. Mater. Res. **10**, 843 (1995).